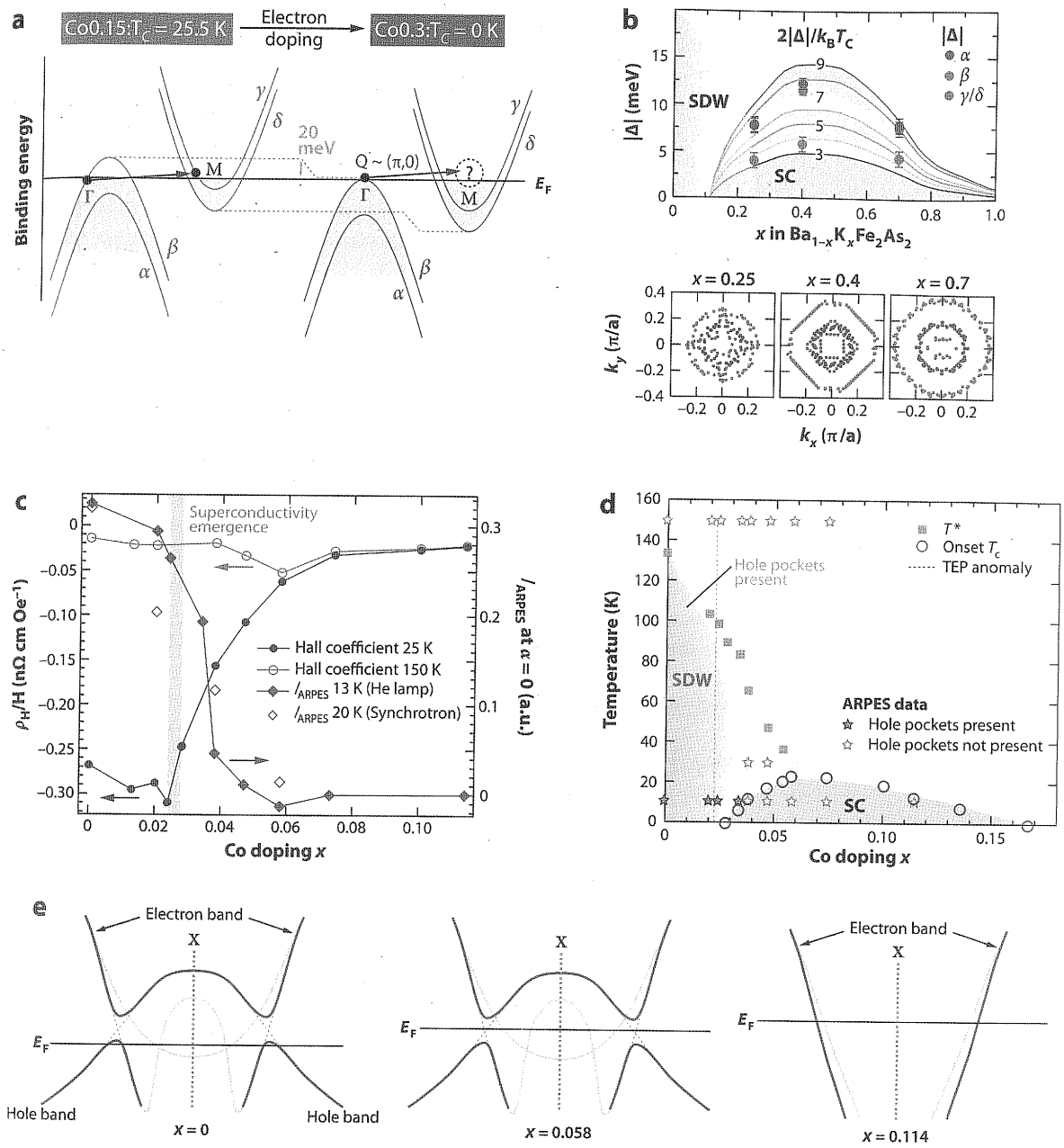

Figure 10

Doping evolution studies. (*a*) Illustration of the suppression of interband scattering with electron doping. (Adapted with permission from Reference 124.) (*b*) Doping dependence of superconducting gap in $Ba_{1-x}K_xFe_2As_2$. (Reprinted with permission from Reference 125. Copyright 2011 by the American Physical Society.) (*c–e*) Doping dependence study of the $Ba(Fe_{1-x}Co_x)_2As_2$ series. (Reprinted with permission from Reference 101. Copyright 2011 Macmillan Publishers Ltd.) (*c*) Comparison of angle-resolved photoemission spectroscopy (ARPES) intensity with Hall coefficients. (*d*) Phase diagram compared with the presence or absence of small hole pockets measured by ARPES. (*e*) Schematic showing a Lifshitz transition near the onset of superconductivity associated with the disappearance of the small hole pockets. Abbreviation: SDW, spin density wave.

spots on the FS at finite doping is more likely due to the lack of AFM band folding, as the SDW transition is suppressed at those dopings, rather than the E_F shifting into the small hybridization gap.

3.5. Outlooks

Even though the iron pnictides are still relatively young players in the field of HTSCs, they have already demonstrated a complexity comparable to that of the cuprates. In this regard, ARPES, with its unique capability to image the electronic structures in energy-momentum space, has been playing an important role in helping us to understand the physics of the pnictides. There are, of course, still many issues to be resolved in this fast developing field.

First of all, how to place the pnictides on the scale of electronic correlation strength still remains an open question. Initial studies of the 1111 and 122 materials have leaned toward weak correlations (86, 126). However, later studies on the 11 chalcogenides have revealed huge mass enhancements and large incoherent spectral weights indicative of strong correlation behavior (127, 128). The latest addition to the family of iron-based superconductors, the 122 chalcogenides (129), which is the first iron-based superconductor family with an insulating parent phase, also seems to indicate strong correlations. To understand such variation of correlation strengths among different pnictide materials one may need to consider the multiorbital nature of the pnictides, as theoretical studies have suggested that both local and itinerant physics may be at play channeled through different orbitals (130), the relative contribution of which may vary with material compositions.

Regarding the issue of superconducting pairing symmetry, so far, all ARPES measurements on the superconducting gap except the most recent one on $BaFe_2(As_{0.7}P_{0.3})_2$ have reported nodeless isotropic gaps. There are still discrepancies with other measurements that report node features in the superconducting gap, such as *c*-axis heat transport on electron-doped $Ba(Fe_{1-x}Co_x)_2As_2$ (131). Such issues may be resolved as crystal quality and experimental conditions are improved, and new exploration is being kept to pace with the ever-expanding material base of the pnictide superconducting family. For the newest 122 chalcogenides, preliminary ARPES studies have shown that the hole bands at Γ sink completely below E_F, leaving only electron pockets on the FS for these effectively electron OD compounds (132–134). This finding is casting doubt on the already widely accepted spin fluctuation induced $s\pm$ pairing mechanism; even though the strong (π, π) scattering between hole bands and electron bands are expected to be significantly suppressed in these materials, they are still capable of superconducting at a T_c as high as 30 K. These are some important issues that ongoing research will help to resolve.

4. GRAPHENE

Carbon, the basis of organic chemistry and life, has an unlimited number of different structures and physical properties due to its flexible bonding structure. The variation in physical properties is intrinsically linked to the dimensionality of the various allotropes ranging from 0D fullerenes to 1D nanotubes, 2D graphene, and 3D graphite (135, 136). Graphene, the 2D allotrope consisting of a single sheet of tightly packed carbon atoms arranged in a honeycomb lattice, has long been studied theoretically for its exotic quantum electrodynamic properties but recent discoveries of isolated free standing sheets of graphene have created a renaissance in carbon-based condensed matter physics. The unusual properties of graphene arise from its relativistic 2D electronic structure. In graphene a formal equivalence is made between the Schrödinger wave equation and the relativistic Dirac equation where the Fermi velocity,

v_F, plays the role of the speed of light (135–142). Graphene's crystal symmetry combined with relativistic physics results in a linear energy dispersion and massless QPs, Dirac fermions, that are degenerate at a single point, the Dirac point, in the BZ. Thus, many quantum electrodynamic properties can appear in graphene but at speeds 300 times smaller than the speed of light (136). This unusual electronic structure is responsible for many interesting transport phenomena including quantum Hall (QH) effect (137, 138) and micrometer-scale ballistic electron transport with mobilities exceeding the best undoped semiconductors (135, 141, 143, 144). Graphene's electronic structure also forms the foundation for superconductivity in other carbon allotropes such as C_{60} crystals, nanotubes, and graphite compounds (145–149). Such exotic properties open new opportunities for quantum computing and virtually lossless, ultrafast electronics on the atomic scale (135, 136, 138, 141).

Graphene consists of carbon atoms arranged in a hexagonal structure with two carbon atoms per unit cell as shown in **Figure 11*a***. Its structural, and electronic, flexibility is due to the robust trigonal in-plane sp^2-derived sigma bands with neighboring carbon atoms and an unaffected p_z orbital extending out of the plane. Although the sigma bands are filled, forming deep valence bands, the p_z orbital is half filled allowing covalent bonding with neighboring carbon atoms forming a π band (136, 139, 150). In graphene the π states are delocalized forming the highest occupied band, π, and the lowest conduction band, π^*. The beauty of graphene is the complexity arising from simplicity. A simple one-orbital tight-binding model, shown in **Figure 11*a***, can accurately describe the single particle band structure $E(k)$ (136, 150, 151). This simple model qualitatively shows the uniqueness of the graphene electronic structure with the π and π^* bands degenerate at the K and K′ points and a near linear dispersion at these Dirac points, E_D. For undoped graphene, the half filled p_z orbitals result in a Fermi level E_F corresponding to E_D making graphene a semimetal because there is vanishing density of states at E_F. The linear dispersion at E_F results in virtually massless carriers traveling at an effective speed of light, $c^* = v_F = \hbar^{-1} dE(k)/dk \sim c/300$.

Although graphene is created every time someone writes a letter using a standard pencil, isolation of individual graphene layers is not trivial. The first successful attempts to isolate a few individual layers of graphitic films were achieved by mechanical exfoliation (repeated peeling) of highly oriented pyrolytic graphite with adhesive tape (143, 156). However, from scientific and technical viewpoints, epitaxial films are necessary to take advantage of graphene's unique electronic properties. Recent advances have demonstrated high-quality epitaxial films suitable for ARPES grown on transition metals and the silicon (0001) and carbon ($000\bar{1}$) faces of SiC (153, 157–159).

The first demonstration of ARPES on thin graphene films utilized in situ growth by thermal desorption of 6H-SiC (159), and the first observed single monolayer ARPES spectrum is shown in **Figure 11*c*** (152). The data beautifully demonstrates the existence of Dirac cones in the electronic structure with a near linear dispersion near E_D shown in **Figure 11*b,c***. **Figure 11*d*** shows a similar electronic structure from a graphene film epitaxially grown on the carbon face of SiC. The first thing to note is that E_D in **Figures 11*c*** and ***d*** are different, emphasizing the influence of the substrate. For both the single layer and multiple graphene sheets grown on the silicon face of SiC, the Dirac point is shifted ~0.4 eV below E_F. This shift is due to the apparent *n*-type doping as the graphene film has a larger electron affinity than the underlying substrate forming a Schottky barrier between the graphene film and the substrate (152, 159–161). Epitaxial films grown on the carbon face of SiC have a nearly ideal band structure as E_D is only ~50 meV above E_F, suggesting a much weaker influence from the substrate (153). In **Figure 11*b*** weak satellite replicas of the Dirac crossing are observed due to the underlying substrate symmetry, whereas the ghostly dispersion replicas in **Figure 11*d*** are not due to the substrate

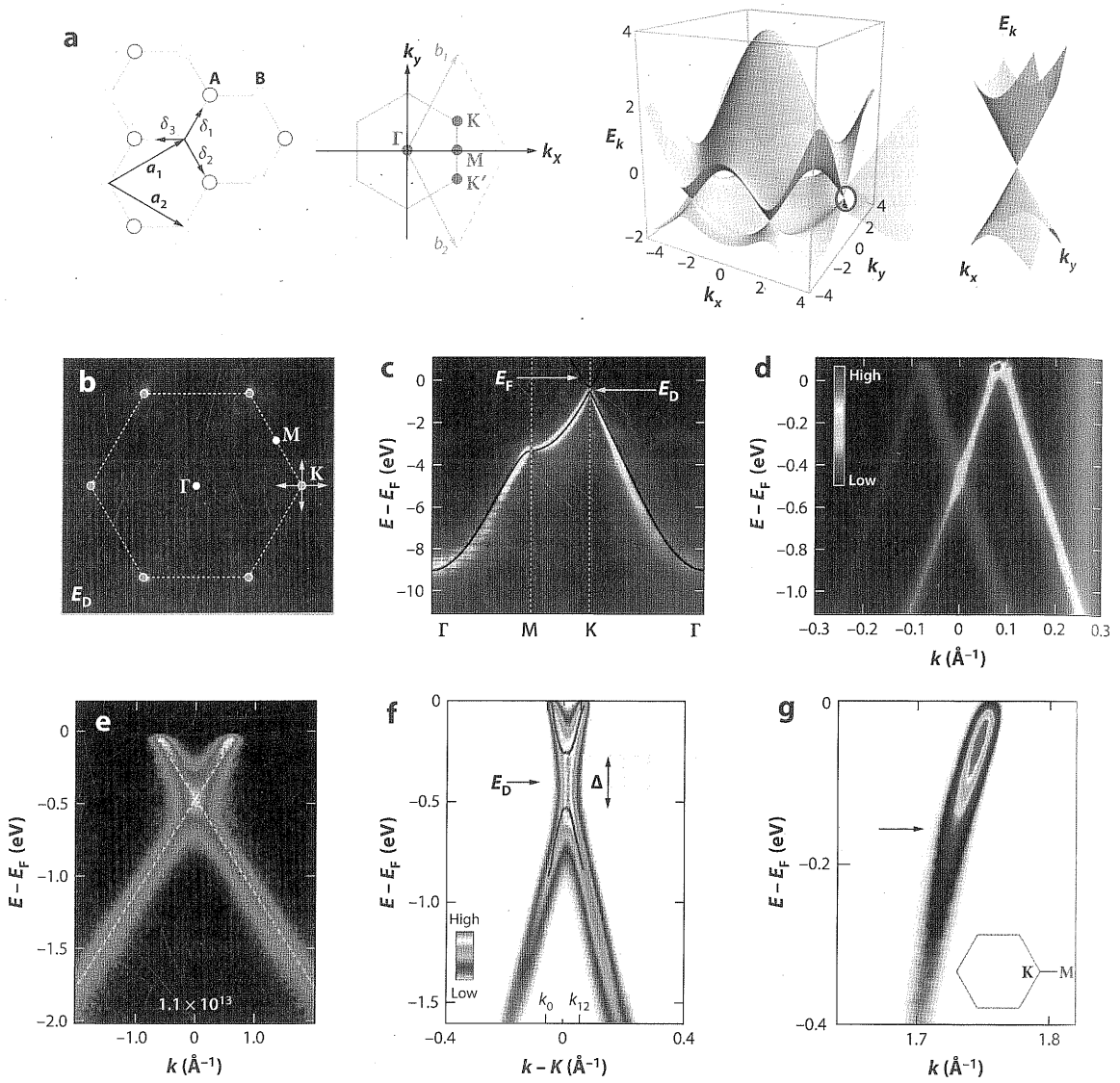

Figure 11

(*a*) Real space and reciprocal space structure of graphene (*left*) and the nearest neighbor tight binding model (*right*) showing the unique linear dispersion of Dirac fermions. (Adapted with permission from Reference 136. Copyright 2009 by the American Physical Society.) (*b*) Constant energy map showing Dirac points at the corner of the Brillouin zone. (Reprinted with permission from Reference 152. Copyright 2007 Macmillan Publishers Ltd.) (*c*,*d*) Electronic structure of single-layer graphene grown on the Si and C faces of SiC, respectively. (*c*, reprinted with permission from Reference 152. Copyright 2007 Macmillan Publishers Ltd. *d*, reprinted with permission from Reference 153. Copyright 2009 by the American Physical Society.) (*e*,*f*) Angle-resolved photoemission spectroscopy spectra of single-layer graphene through K-point showing different data interpretations. (*e*, reprinted with permission from Reference 152. Copyright 2007 Macmillan Publishers Ltd. *f*, reprinted with permission from Reference 154. Copyright 2007 Macmillan Publishers Ltd.) (*g*) High-resolution spectra of single-layer graphene emphasizing kink due to many-body effects. (Reprinted with permission from Reference 155. Copyright 2008 Macmillan Publishers Ltd.)

but from single monolayers electronically decoupled from adjacent monolayers due to a ~2° rotational stacking disorder, yielding single-layer transport properties from a few-layers-thick films (153).

The technological potential of graphene lies in the ability to dramatically tune the carrier concentration with the application of an electric field. For the ideal graphene-based electronic device, a single graphene layer is desired with a gap at the Dirac point so that switching can be achieved with an applied gate voltage. There are two possible ways to create a gap at E_D in a single layer of graphene. The first is to break translational symmetry and the second is to break the sublattice symmetry by making the A and B atomic sites inequivalent, rehybridizing the π and π^* bands. However, there are issues that need to be resolved before such a device could become a reality. Interactions between the substrate and graphene film need to be controlled, and possible many-body interactions arising from relativistic, virtually massless charge carriers need to be understood. Although ARPES is the ideal tool to study both effects on graphene's electronic structure, there is currently a lack of consensus in the ARPES community and still much to learn about the basic electronic structure of graphene (152, 154, 167–169). One group proposes a 0.26 eV gap exists at E_D owing to a substrate-induced lifting of the A,B sublattice symmetry as shown in **Figure 11*f*** (154); a second group proposes that there is no gap, but novel electron-plasmon coupling renormalizing the band dispersion and carrier scattering rate creating the subtle band features observed near E_D as shown in **Figure 11*e*** (152). A gap is also found in single-layer graphene films grown on an Au intercalated Ru(0001) surface and, once again, a lifting of the A,B sublattice symmetry is proposed (170, 171).

The thickness of the graphene films is easily identified in ARPES spectra. As the number of graphene layers increases, the number of π bands observed increases owing to weak interlayer coupling between the graphene layers as shown in **Figure 12*a,b*** (162, 163). Films one to four layers thick can easily be identified, whereas films thicker than four layers tend to have graphite bulk–like electronic structure. In a freestanding graphene film, the A and B atomic sites are equivalent, resulting in degenerate π bands at the K and K′ points in the BZ. However, in graphite this equivalence is lifted due to the weak interlayer coupling and the fact that there is a carbon atom directly under the A site, whereas there is none below the B site. This breaking of the sublattice symmetry results in a gap at the Dirac point, and such a gap is readily apparent in the bilayer and thicker graphene films as shown in **Figure 12*c***. In addition, there are two possible stacking sequences for graphene films, Bernal (*ABA*...) and rhombohedral (*ABCA*...), and the energy difference between the two is very small (172). Although bulk graphite and graphene films grown on the carbon face of SiC typically form with the Bernal stacking sequence (162), both scenarios are identified in the thin graphene films grown on the silicon face of SiC (163). The dimensionality of the 2D single-layer and 3D multiple-layer thick films is apparent by the change in k_z dispersion demonstrated in **Figure 12*b***.

To better understand the characteristics of graphene films with different carrier concentrations, chemical doping with alkali metals (152, 160, 173), hydrogen (166), and NO_2 (165) is used to control the band filling and electronic structure. Potassium doping results in an *n*-type rigid band shift of the π bands and alters the existence and size of an energy gap in bilayer graphene, as shown in **Figure 12*c*** (160). The ultimate goal is to generate an insulating graphene sheet so that transport can be controlled with an electric field. Two different routes for creating a metal-to-insulator transition in graphene have been realized, but for different physical reasons. **Figure 12*e*** shows bilayer graphene is hole-doped with the addition of NO_2 (165). A rigid band shift pushes the gap at E_D to the Fermi level, thus generating an insulating film. Alternatively, **Figure 12*f*** shows H-doped graphene where there is a marked reduction in the FS area with little effect on E_D (166). Simultaneous transport measurements reveal an insulating film

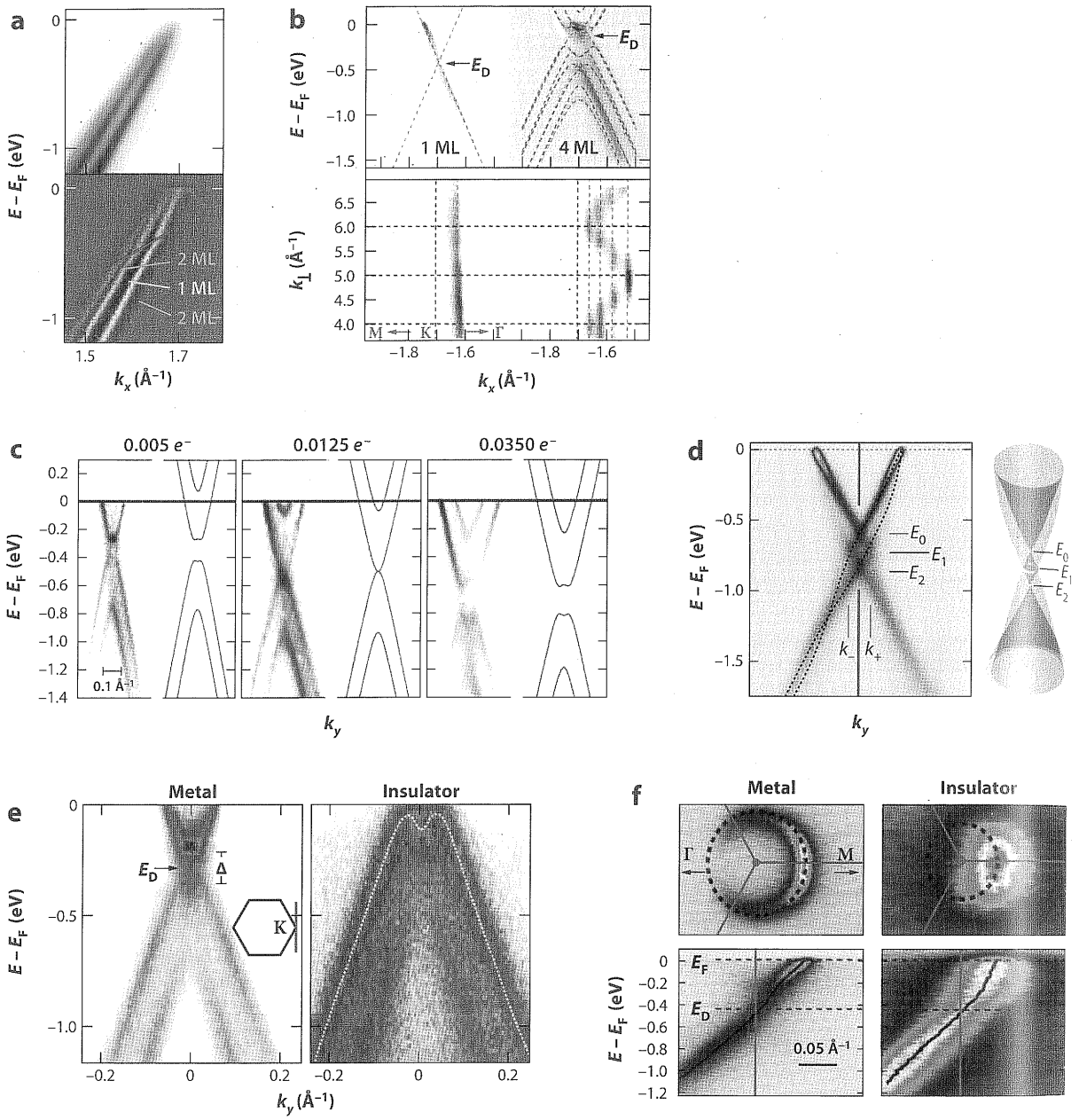

Figure 12

(*a*,*b*) ARPES spectra for multiple layers of graphene grown on the C and Si faces of 6HSiC, respectively. (Reprinted with permission from References 162 and 163. Copyright 2007 and 2010, respectively, by the American Physical Society). (*c*) Control of bilayer graphene band structure by potassium doping. (From Reference 160. Reprinted with permission from AAAS.) (*d*) Plasmarons observed in single monolayer graphene electronic structure. (From Reference 164. Reprinted with permission from AAAS.) (*e*) Graphene metal-to-insulator transition (MIT) by hole doping with NO_2. (Reprinted with permission from Reference 165. Copyright 2008 by the American Physical Society.) (*f*) Graphene MIT via Anderson localization by doping with H. (Reprinted with permission from Reference 166. Copyright 2009 by the American Physical Society.)

with a visible FS and a breakdown of the QP picture where the authors propose Anderson localization to explain their unusual results.

Investigating many-body interactions with high-resolution scans, one of which is shown in Figure 11*g*, reveals the roles of electron-phonon and electron-electron interactions below E_F, due to a Kohn anomaly and soft A_{1g} phonon mode (152, 155). High-resolution studies of potassium-doped single-layer films, shown in Figure 12*d*, reveal plasmarons, new electronic composite states of bound charge carriers with plasmons (164).

Clearly, there is considerable work still to be done to fully understand the electronic structure of graphene. Samples are now approaching pristine wafer-sized graphene sheets (174), and improved understanding will follow the improved films. Graphene shows immense potential for device applications but there is much to learn about the electronic structure and many-body effects in such a 2D relativistic Dirac fermion system.

5. TOPOLOGICAL INSULATORS

In condensed matter physics, different states of matters are usually classified by the spontaneous breaking of symmetries (175). As examples, a crystal breaks translational symmetry; a magnet breaks rotational symmetry; and a superconductor breaks the more subtle gauge symmetry. The first new state that does not have spontaneous broken symmetry was the QH state discovered in 1980 (176). In this state, the bulk of the 2D sample is insulating, and the dissipationless electric current can flow only along the sample edge, giving rise to a quantized Hall effect. The QH state is topologically distinct from all previously known states of matter. Recently, a new class of topological state, TIs, have emerged. TIs represent a novel quantum matter with a bulk gap and an odd number of relativistic Dirac fermions on the surface (177). This state is topologically distinct from all other known states of matter, including the QH state.

Soon after the theoretical prediction (178), the 2D TI state, or the quantum spin Hall (QSH) state, was experimentally observed in the HgTe quantum wells (179). In this state (180, 181), there is an insulating gap in the bulk and gapless states at the edge where electrons with opposite spins counter-propagate (Figure 13*a*), forming a single massless Dirac fermion at the edge (Figure 13*b*) and the crossing of their dispersion branches at a time reversal invariant point (Dirac point) is protected by the TRS (182).

In 3D, a TI has a bulk gap and its conduction electrons flow only on the surface (2D), with their electron spin polarization locked to the momentum (Figure 13*c*), forming a cone-shape

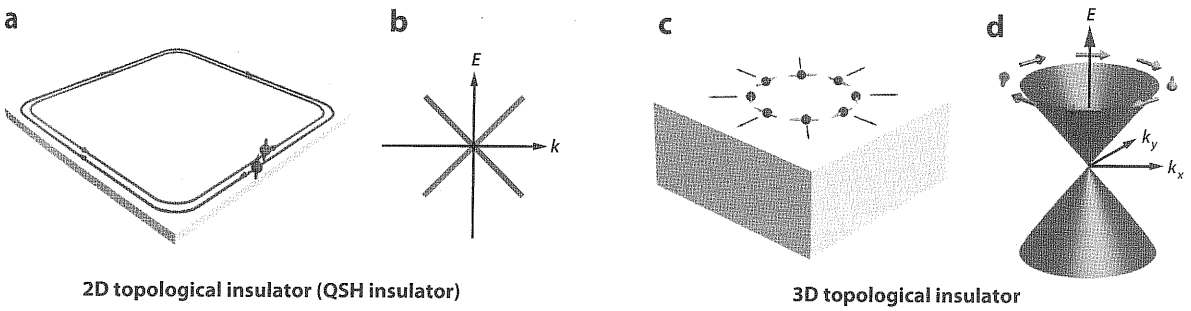

Figure 13

(*a*) In a 2D quantum spin Hall (QSH) insulator, the electric current flows at the edge of the 2D sample, forming two branches of the linearly dispersed band as shown in panel *b*. (*c*) For a 3D topological insulator, the spin of the surface electron is "locked" to its momentum, forming a cone-shape dispersion with helical spin polarization as illustrated in panel *d*.

dispersion; a Dirac cone (**Figure 13*d***) with the Dirac point resides at the time reversal invariant point (183–186). Several families of 3D TIs were soon predicted, including the $Bi_{1-x}Sb_x$ alloy ($x = 0.07{\sim}0.22$) (187), $V_2 - VI_3$ binary compounds (Bi_2Te_3, Bi_2Se_3 and Sb_2Te_3) (188), $III–V–VI_2$ ternary compounds ($TlBiSe_2$) (189, 190), and many Heusler alloys (191, 192).

Unlike the 2D case, where the electric transport experiments played a vital role in confirming the QSH state (179), transport experiments are hard to use to determine the 3D TI materials, not only because the contribution from the surface state is much smaller in the conductivity and the challenge to distinguish bulk and surface contributions, but also because the 2D surface state of 3D TI does not lead to the complete suppression of the resistance as does the 1D edge state in the 2D case (185).

ARPES, however, has the capability to probe the surface state structure of 3D TIs directly. With the ability to examine the k_z dependence of the band structure by photon-energy-dependence measurements, ARPES can easily separate the bulk and surface contributions. It is thus an ideal technique for studying the unique electronic structure of 3D TIs. Furthermore, the integration of the spin-detector to the ARPES spectrometer makes it possible to study the helical spin-structure of TIs. In the rest of this section, we use a few examples to demonstrate the successful application of ARPES in 3D TIs.

5.1. Bi_xSb_{1-x} Alloy

The first practical 3D TI candidate was proposed by Fu & Kane on $Bi_{1-x}Sb_x$ alloy (187). Pure bismuth is a semimetal with strong spin-orbital coupling, and the overlap between the conduction bands (around L points) and valence bands (around T points) leads to simultaneous existence of electron and hole pockets. Substituting bismuth by antimony changes the band structure, leading to the downshift of the T and L_s bands and the upshift of the L_a band (**Figure 14*a***). With the increase of antimony concentration, the direct gap at the L points gets smaller and vanishes at $x \approx 0.04$, then becomes negative with further antimony doping. When $x \geq 0.07$, the T band falls below the L_s band; thus, the alloy becomes a semiconductor with an inverted band gap between the L_a and L_s bands. The situation persists till $x \approx 0.22$, when the H band crosses the L_s band, making the system a semimetal again. Thus, within the range $0.07 < x < 0.22$, the $Bi_{1-x}Sb_x$ alloy is a semiconductor with the inverted band at L points. Fu & Kane predicted (187) that within this region, the system is a strong 3D TI, featuring an odd number of the crossing of the surface state through the E_F.

The ARPES experiments on $Bi_{1-x}Sb_x$ alloy were soon carried out by Hsieh et al. (193); in their work, the surface state band (SSB) was shown to cross E_F five times (**Figure 14*b***), and their subsequent spin-resolved experiments (194) further showed the spin of the SSBs indeed correlate with the electron momentum (**Figure 14*c***), indicating that the $Bi_{1-x}Sb_x$ is a 3D TI with a bulk gap ~50 meV.

5.2. V_2–VI_3 Family of Single Dirac Cone Topological Insulators

Although the $Bi_{1-x}Sb_x$ alloy shows an odd number of Fermi-crossings, the complicated band structure (five E_F crossings) and the small energy gap (~50 meV) motivate the search for simpler 3D TI materials, ideally with a single Dirac fermion on the surface—similar to the hydrogen atom in the atomic physics—to make the topological properties most prominent in these materials and simplify the application schemes.

After theoretical investigations and ab initio calculations, several compounds from the $V_2 - VI_3$ family materials were proposed (188) to be large-gap single Dirac cone TIs, including

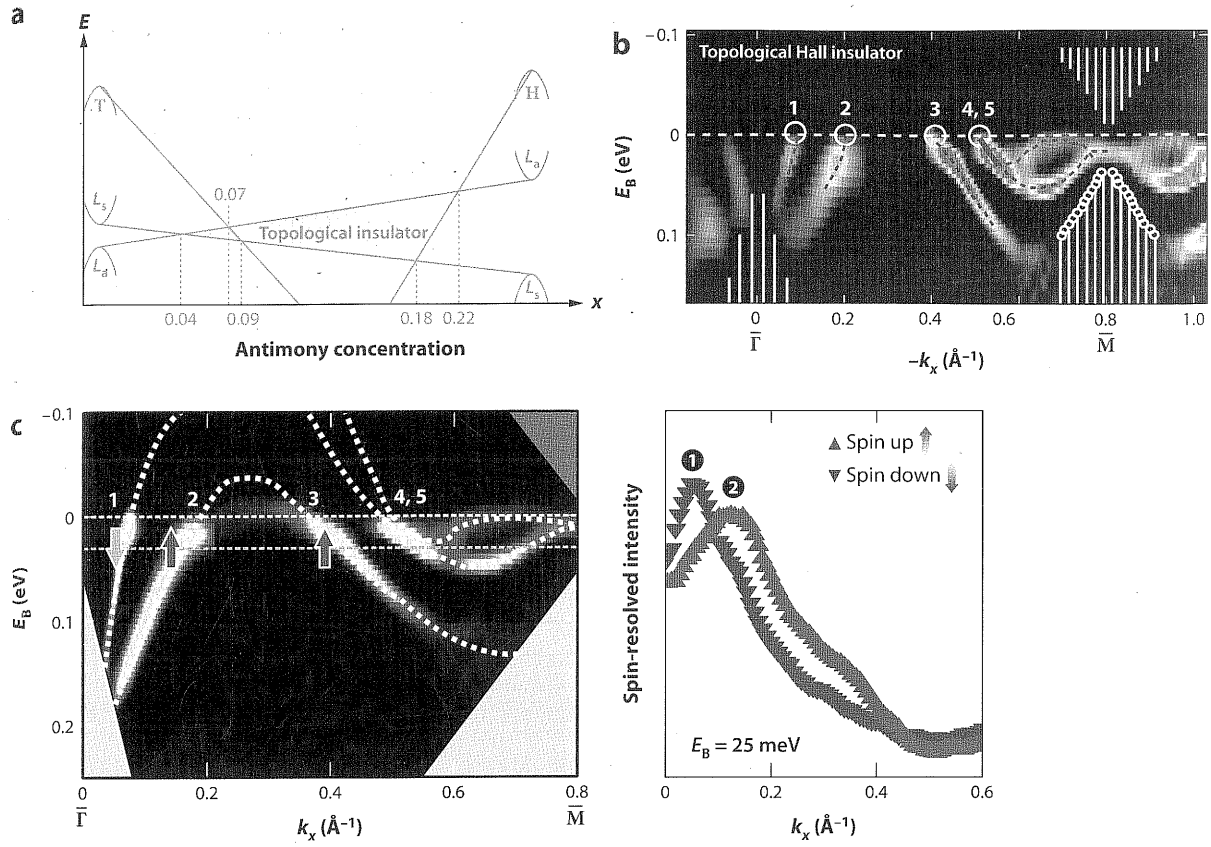

Figure 14

(*a*) Schematic of the band evolution of $Bi_{1-x}Sb_x$ as a function of x. (Reprinted with permission from Reference 187. Copyright 2007 by the American Physical Society.) (*b*) The surface-band-dispersion (second-derivative) image of $Bi_{0.9}Sb_{0.1}$ along the Γ-M direction, showing five E_F crossings from Γ to M (*yellow circles*). The shaded white area shows the projection of the bulk bands based on angle-resolved photoemission spectroscopy data, as well as a rigid shift of the tight binding bands to sketch the unoccupied bands above the Fermi level. (Reprinted with permission from Reference 193. Copyright 2008 Macmillan Publishers Ltd.) (*c*) Surface band dispersion image along the Γ-M direction (*left panel*) with the spin polarization (*right panel*). (From Reference 194. Adapted with permission from AAAS.)

Bi_2Te_3, Bi_2Se_3, and Sb_2Te_3. The physics in this family of materials can be understood by a simple effective model (188). Basically, the strong interaction caused the inversion of the bismuth and selenium p_z orbitals, resulting in a single Dirac cone centered at the Γ-point of the surface BZ. This simplicity makes this family of materials an ideal candidate for realizing the many proposed topological phenomena, such as the magneto-electric effect (185). Furthermore, the predicted large bulk gap makes them potential candidates for high-temperature spintronics applications.

ARPES studies soon confirmed the theoretical prediction of a single Dirac cone for all three proposed materials (195–197), with a gap of 165 meV and 200 meV for Bi_2Te_3 (195) and Bi_2Se_3 (198), respectively, which is much larger than that of $Bi_{1-x}Sb_x$ alloy (~50 meV) (193). Furthermore, by introducing both surface or bulk dopants (**Figure 15***g*,*h*), the E_F of 3D TIs can be freely tuned through the bulk gap, making the materials in both *p*- and *n*-type dopings, or in the topological transport point. This tunability makes many applications feasible such as

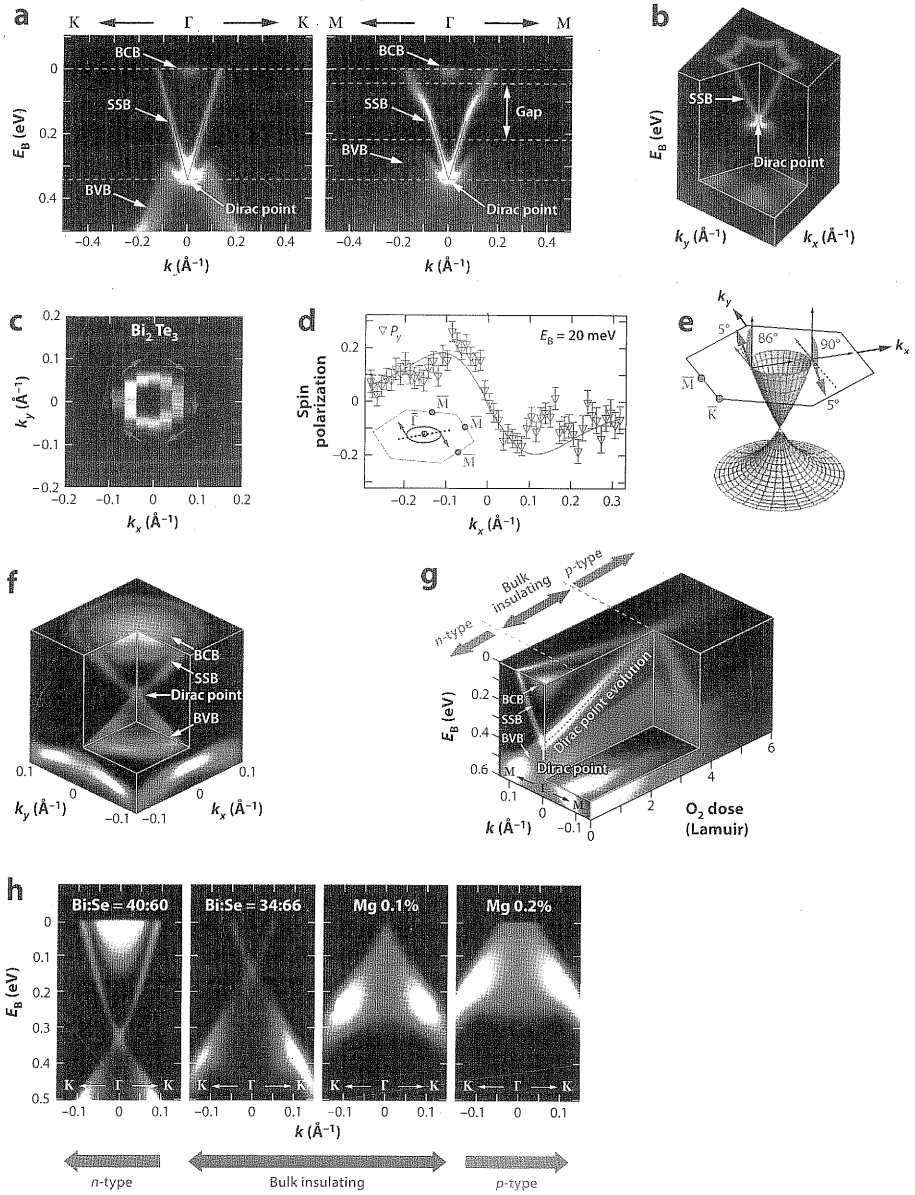

Figure 15

(*a*) Angle-resolved photoemission spectroscopy (ARPES) measurements of band dispersions from Bi_2Te_3 along the K-Γ-K and M-Γ-M directions. (Adapted from Reference 195.) The broad bulk conduction band (BCB), the bulk valance band (BVB), and the sharp V-shape linear dispersion from the Dirac surface state band (SSB) are labeled. The apex of the V-shape SSB dispersion is the Dirac point. (*b*) 3D illustration of the dispersion of $(Bi_{0.9933}Sn_{0.0067})_2Te_3$. (*c–e*) Spin-resolved photoemission data from Bi_2Te_3 (199). (*c*) Fermi surface map; (*d*) measured *y*-component of spin-polarization along the Γ-M direction; and (*e*) fitted spin polarization vector $P(S_x, S_y, S_z)$ demonstrating the topological helicity of the Dirac cone. (*f,g*) ARPES measurements of Bi_2Se_3 family (198). (*f*) 3D band structure of Bi_2Se_3. (*g*) Evolution of the band structure (along the M-Γ-M direction) by photon-assisted surface doping with O_2. Light blue dashed line traces the upward shift of the Dirac point with the O_2 doping, whereas green dashed lines indicate the dosages that separate the three doping regions. (*h*) With bulk doping, the band structure evolves from the *n*-type (*far left panel*, as grown Bi_2Se_3), through the bulk insulating region (*inner left panel*, $Bi_{1.7}Se_{3.3}$), and the topological transport point [*inner right panel*, $(Bi_{0.999}Mg_{0.001})_2Se_3$], to *p*-type [*far right panel*, $(Bi_{0.998}Mg_{0.002})_2Se_3$].

topological *p-n* junction. The spin polarization of the surface state was also investigated by the spin-resolved ARPES (**Figure 15*c–e***), confirming the unique signature of the spin-momentum locking in 3D TIs.

Despite the broad agreement with the theoretical prediction, there is a distinction between the hexagram FS of the measured SSB and a circular FS from the simple prediction. Motivated by this difference, Fu (199) added an additional term into the surface Hamiltonian and explained the hexagonal warping effect. Furthermore, this revised model has observable predictions on the surface QP interference, which was soon observed by scanning tunneling microscopy (200).

5.3. Effects of Nonmagnetic and Magnetic Impurities

In the presence of TRS, the surface Dirac fermions of TIs are protected, leading to a degeneracy at the Dirac point that connects the upper and lower surface Dirac cones (**Figure 16*b***), even if the system is perturbed by nonmagnetic impurities (**Figure 16*a***). This is again confirmed by the ARPES measurements (**Figure 16*c,d***) on nonmagnetically doped Bi_2Se_3, where the band structures of intrinsic and Tl-doped samples are shown, respectively (see Reference 198 for more examples). In both cases, the continuity at the Dirac point is indicated by the strong spectral intensity (**Figure 16*c,d***, left subpanels) and the single peak structure of the EDC at the Dirac point (**Figure 16*c,d***, right subpanels). In **Figure 16*d***, the charge doping effect of Tl is clearly seen by the dramatic shift of E_F into the bulk gap. Nonetheless, the topology of the surface Dirac cone remains the same with a continuous Dirac point.

The TRS protection of the Dirac point can be lifted by magnetic dopants (**Figure 16*e***), resulting in a gap that separates the two branches of the Dirac cone (**Figure 16*f***). This is illustrated in the band structure (**Figure 16*g***) of an Fe-doped sample. Unlike nonmagnetically doped cases, the SSB dispersion at the Dirac point is broken, as indicated by the suppressed intensity regions in the spectral density plots (**Figure 16*g***, left subpanels) and the twin-peak structure around the Dirac point in the EDC plots (**Figure 16*g***, right subpanels).

Given the SSB gap formation at the Dirac point with broken TRS, we can further realize the insulating massive Dirac fermion state, a state that is capable of hosting many novel topological phenomena (185, 202–204). To do so, we need to tune the E_F into this gap. This can be achieved by manganese doping because manganese has one less valence electron than bismuth; thus, it not only introduces magnetic moments into the system but also naturally dopes holes into the sample to lower the E_F. The measurements on an OP sample clearly show that the E_F resides right inside the SSB gap (**Figure 16*h***, left panel), which is at least 7 meV (**Figure 16*h***, right panel). Thus, the insulating massive Dirac fermion state is achieved.

5.4. Other Topological Insulators and Perspective

Despite the exciting progress made in the past three years, the field of TIs is still early in its development. Many of the amazing topological effects and their potential applications are limited by the nonideal properties of current TIs. For example, to date, the 2D QSH effect was discovered only in the HgTe/CdTe quantum well system, and the small gap (20 meV) of the HgTe/CdTe quantum well prevents it from being used for high (room) temperature applications. In the 3D case, though the Bi_2Te_3/Bi_2Se_3 family of materials has a bulk gap of up to 200 meV, the layered nature and the van der Waals force bonding between quintile layers make it difficult to shape into the desired forms for transport measurement and applications; and foreign atoms can easily get into the interstitial space between quintuple layers, introducing

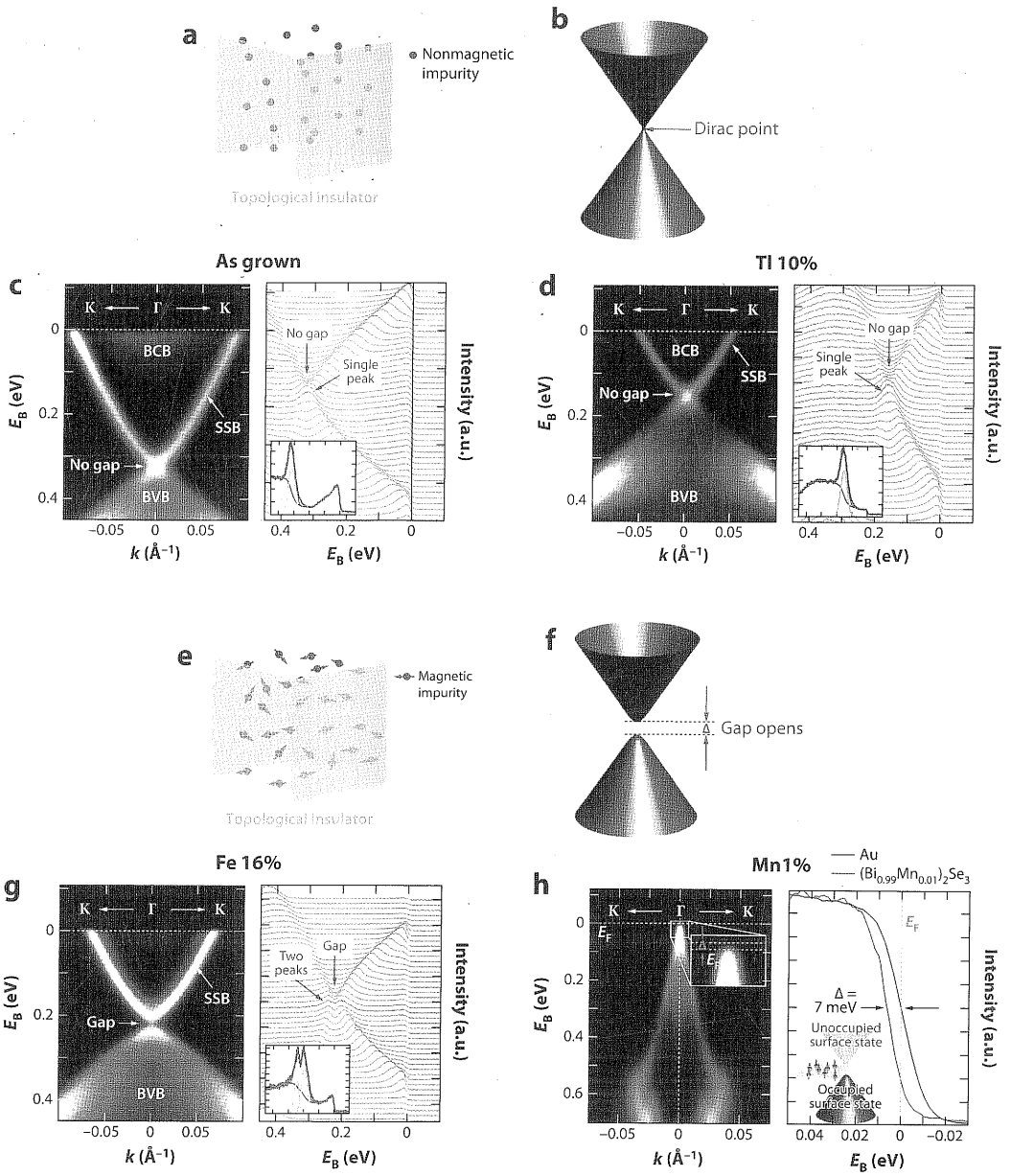

Figure 16

(*a*,*b*) Schematic of nonmagnetically doped topological insulator (TI) with a Dirac point connecting the upper and lower Dirac cones as in the undoped case. (*c*) Band structure along the K-Γ-K direction of undoped Bi_2Se_3. (*d*) Band structure for a Tl-doped sample, $(Bi_{0.9}Tl_{0.1})_2Se_3$. The Dirac point remains continuous. (*e*,*f*) Schematic of magnetically doped TI with a broken Dirac point and a gap separating the upper and lower Dirac cones. (*g*) Band structure of $(Bi_{0.84}Fe_{0.16})_2Se_{3.7}$. At the Dirac point, the reduced spectral intensity (*left*) and the twin-peak structure in the energy distribution curves (EDCs) (*right*) indicate a gap formation. (*h*) Left panel: ARPES spectra along the K-Γ-K direction of $(Bi_{0.99}Mn_{0.01})_2Se_3$ showing the E_F inside the surface Dirac gap. Inset: Close-up of the dispersion in the vicinity of E_F, indicating a gap between the leading edge of the surface state band (SSB) and E_F. Vertical white dashed line shows the location of the EDC plotted in the right panel. Right panel: Comparison between the Γ-point EDC (*blue*) and E_F, which shows a leading-edge gap of 7 meV. A reference EDC from a polycrystalline Au sample whose leading edge, as expected, coincides with E_F is shown in red. Abbreviation: BVB, bulk valence band. (Panels adapted from Reference 198.)

undesired impurities and charge dopings (195, 198, 205). Thus, one would like to search for more TI materials with better chemical, physical, and electronic properties.

In **Figure 17**, we give two examples to demonstrate the recent effort in the search for new TIs in $III - V - VI_2$ family compounds (206). From **Figure 17*a–c***, the characteristic single Dirac cone at the Γ-point immediately indicates the nontrivial topological nature of these two compounds. In **Figure 17*a***, $TlBiSe_2$ shows a bulk gap of ~200 meV, which is similar to that of Bi_2Se_3. However, $TlBiSe_2$ has much better physical properties than the Bi_2Se_3 family of compounds due to the covalent bonding between atomic layers, which is much stronger (189, 190) than the van der Waals force that bonds quintuple layer units of Bi_2Te_3 or Bi_2Se_3 (188), making these materials much more favorable for other measurements and applications.

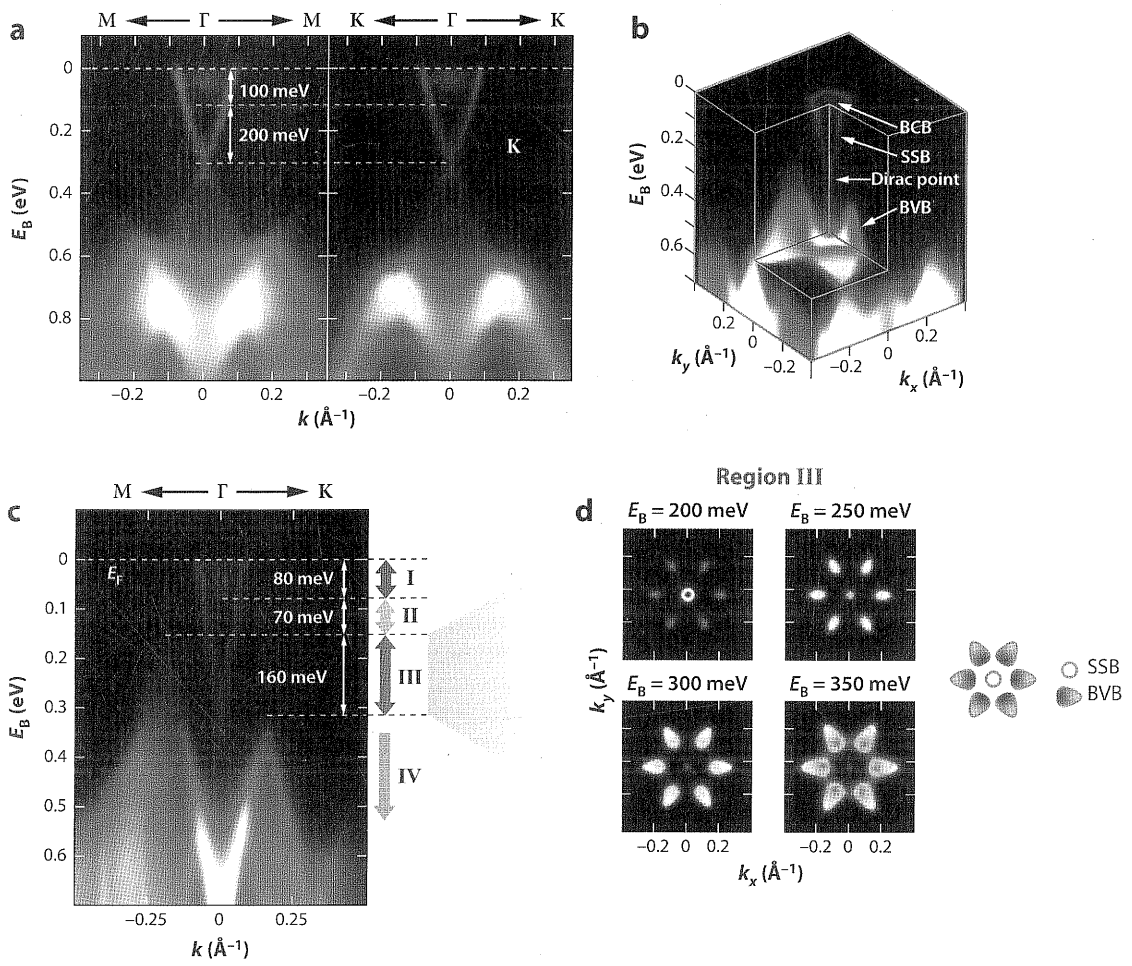

Figure 17

(*a*) Dispersions of an *n*-type topological insulator $TlBiSe_2$ along two high-symmetry directions, indicating a bulk gap of ~200 meV and a single-surface Dirac fermion around the Γ-point. (*b*) 3D band structure of $TlBiTe_2$ around Γ. (*c*) Combined dispersion along M-Γ-K direction. Four regions defined by characteristic energy positions are labeled as I, II, III, and IV, respectively. (*d*) Four constant energy plots of the band structure from region III defined in panel *c*, showing the six characteristic bulk valance band (BVB) hole pockets outside the surface state band (SSB) pocket, as demonstrated in the diagram on the far right. Abbreviation: BCB, bulk conduction band. (Panels adapted from Reference 206.)

Besides having the Dirac surface state, another compound, $TlBiTe_2$, was reported to show a superconducting transition at $T_c \sim 0.14$ K when p-doped (207) to a carrier density of 6×10^{20}. At this doping, the E_F of the system is ~150 meV below the bulk conduction band bottom and resides in region III, where the FS geometry is characterized by a ringlike SSB FS and six surrounding p-type bulk pockets (**Figure 17***d*). This naturally indicates that the bulk superconductivity of p-type $TlBiTe_2$ originates from the six leaf-like bulk pockets, and in the superconducting state, the surface state can become superconducting owing to the proximity effect. For such a superconductor, it has been proposed (208) that each vortex line has two Majorana zero modes related by the TRS, making it a candidate for the long sought after topological superconductors (which will be discussed below) and suitable for the topological quantum computation (209).

Following these discoveries in 2D and 3D materials, TIs have grown as one of the most intensively studied fields in condensed matter physics. The swift development of TIs also inspires the study of other topological states. Quantum anomalous Hall insulators (210) and topological superconductors (208) are two such examples.

In a quantum anomalous Hall insulator, spontaneous magnetic moments and spin-orbit coupling combine to give rise to a topologically nontrivial electronic structure, leading to the quantized Hall effect without an external magnetic field. The quantum anomalous Hall effect is the last quantized effect in the Hall effect family besides the Hall effect and the spin Hall effect. Given the large separation between the conducting channels, the back scattering of the electrons is further suppressed, leading to the promising low-power applications.

A topological superconductor has a pairing gap in the bulk and topologically protected surface state consisting of Majorana fermions (208). Unlike Dirac fermions in TIs that can have the form of particles or holes, Majorana fermions are their own antiparticles (208, 211–214). The simplest 3D topological superconductor consists of a single Majorana cone on the surface, containing half the degree of freedom of the Dirac surface state of a single cone 3D TI. This fractionalization of the degree of freedom introduces quantum nonlocality and is essential to the topological quantum computing based on Majorana fermions (209).

The study of these new quantum materials will not only be of great scientific interest, but also provide new opportunities for novel applications. We expect that the ARPES technique will continue to play a leading role in the research on novel topological quantum materials and greatly contribute to the development in this new frontier.

DISCLOSURE STATEMENT

The authors are not aware of any affiliations, memberships, funding, or financial holdings that might be perceived as affecting the objectivity of this review.

ACKNOWLEDGMENTS

This work is supported by U.S. Department of Energy, Office of Basic Energy Sciences, Materials Sciences Division.

LITERATURE CITED

1. Tallon JL, Loram JW. 2001. *Physica C* 349:53–68
2. Birgeneau RJ, Stock C, Tranquada JM, Yamada K. 2006. *J. Phys. Soc. Jpn.* 75:111003

3. LeBoeuf D, Doiron-Leyraud N, Vignolle B, Sutherland M, Ramshaw BJ, et al. 2011. *Phys. Rev. B* 83:054506
4. Balédent V, Haug D, Sidis Y, Hinkov V, Lin CT, Bourges P. 2011. *Phys. Rev. B* 83:104504
5. Damascelli A, Hussain Z, Shen ZX. 2003. *Rev. Mod. Phys.* 75:473–542
6. Shen KM, Ronning F, Meevasana W, Lu DH, Ingle NJC, et al. 2007. *Phys. Rev. B* 75:075115
7. Mahan GD. 1993. *Many-Particle Physics*. New York: Plenum, 2nd ed.
8. Pothuizen JJM, Eder R, Hien NT, Matoba M, Menovsky AA, Sawatzky GA. 1997. *Phys. Rev. Lett.* 78:717–20
9. Shen KM, Ronning F, Lu DH, Lee WS, Ingle NJC, et al. 2004. *Phys. Rev. Lett.* 93:267002
10. Mannella N, Yang WL, Tanaka K, Zhou XJ, Zheng H, et al. 2007. *Phys. Rev. B* 76:233102
11. Lanzara A, Bogdanov PV, Zhou XJ, Kellar SA, Feng DL, et al. 2001. *Nature* 412:510–14
12. Bogdanov P, Lanzara A, Kellar SA, Zhou XJ, Lu ED, et al. 2000. *Phys. Rev. Lett.* 85:2581–84
13. Zhou XJ, Cuk T, Devereaux T, Nagaosa N, Shen ZX. 2007. In *Handbook of High-Temperature Superconductivity*, pp. 87–144. New York: Springer
14. Cuk T, Lu DH, Zhou XJ, Shen ZX, Devereaux TP, Nagaosa N. 2005. *Phys. Stat. Sol. (b)* 242:11–29
15. Johnston S, Lee WS, Chen Y, Nowadnick EA, Moritz B, et al. 2010. *Adv. Condens. Matter Phys.* 2010:968304
16. Cuk T, Baumberger F, Lu DH, Ingle N, Zhou XJ, et al. 2004. *Phys. Rev. Lett.* 93:117003
17. Kaminski A, Randeria M, Campuzano JC, Norman MR, Fretwell H, et al. 2001. *Phys. Rev. Lett.* 86:1070–73
18. Johnson PD, Valla T, Fedorov AV, Yusof Z, Wells BO, et al. 2001. *Phys. Rev. Lett.* 87:177007
19. Zhou XJ, Shi J, Yoshida T, Cuk T, Yang WL, et al. 2005. *Phys. Rev. Lett.* 95:117001
20. Devereaux T, Cuk T, Shen ZX, Nagaosa N. 2004. *Phys. Rev. Lett.* 93:117004
21. Borisenko SV, Kordyuk AA, Kim TK, Koitzsch A, Knupfer M, et al. 2003. *Phys. Rev. Lett.* 90:207001
22. Gromko AD, Fedorov AV, Chuang YD, Koralek JD, Aiura Y, et al. 2003. *Phys. Rev. B* 68:174520
23. Gweon GH, Sasagawa T, Zhou SY, Graf J, Takagi H, et al. 2004. *Nature* 430:187--90
24. Iwasawa H, Douglas JF, Sato K, Masui T, Yoshida Y, et al. 2008. *Phys. Rev. Lett.* 101:157005
25. Meevasana W, Zhou XJ, Sahrakorpi S, Lee WS, Yang WL, et al. 2007. *Phys. Rev. B* 75:174506
26. Moritz B, Johnston S, Devereaux TP. 2010. *J. Electron Spectrosc. Relat. Phenom.* 181:31–34
27. Liu G, Wang G, Zhu Y, Zhang H, Zhang G, et al. 2008. *Rev. Sci. Instrum.* 79:023105
28. Vishik IM, Lee WS, Schmitt F, Moritz B, Sasagawa T, et al. 2010. *Phys. Rev. Lett.* 104:207002
29. Plumb NC, Reber T, Koralek JD, Sun Z, Douglas JF, et al. 2010. *Phys. Rev. Lett.* 105:046402
30. Rameau JD, Yang HB, Gu GD, Johnson PD. 2009. *Phys. Rev. B* 80:184513
31. Anzai H, Ino A, Kamo T, Fujita T, Arita M, et al. 2010. *Phys. Rev. Lett.* 105:227002
32. Johnston S, Vishik IM, Lee WS, Schmitt F, Uchida S, et al. 2011. arXiv:1101.1302
33. Lee WS, Meevasana W, Johnston S, Lu DH, Vishik IM, et al. 2008. *Phys. Rev. B* 77:140504
34. Lee WS, Tanaka K, Vishik IM, Lu DH, Moore RG, et al. 2009. *Phys. Rev. Lett.* 103:067003
35. Meevasana W, Ingle NJC, Lu DH, Shi JR, Baumberger F, et al. 2006. *Phys. Rev. Lett.* 96:157003
36. He H, Bourges P, Sidis Y, Ulrich C, Regnault LP, et al. 2002. *Science* 295:1045–47
37. Xia J, Schemm E, Deutscher G, Kivelson SA, Bonn DA, et al. 2008. *Phys. Rev. Lett.* 100:127002
38. Li Y, Baledent V, Barisic N, Cho Y, Fauque B, et al. 2008. *Nature* 455:372–75
39. Loeser AG, Shen ZX, Dessau DS, Marshall DS, Park CH, et al. 1996. *Science* 273:325–29
40. Norman MR, Ding H, Randeria M, Campuzano JC, Yokoya T, et al. 1998. *Nature* 392:157–60
41. Kugler M. 2001. *Phys. Rev. Lett.* 86:4911–14
42. Kanigel A, Chatterjee U, Randeria M, Norman MR, Koren G, et al. 2008. *Phys. Rev. Lett.* 101:137002
43. Yoshida T, Hashimoto M, Ideta S, Fujimori A, Tanaka K, et al. 2009. *Phys. Rev. Lett.* 103:037004
44. Lee WS, Vishik IM, Tanaka K, Lu DH, Sasagawa T, et al. 2007. *Nature* 450:81–84
45. Tanaka K, Lee WS, Lu DH, Fujimori A, Fujii T, et al. 2006. *Science* 314:1910–13
46. Kondo T, Khasanov R, Takeuchi T, Schmalian J, Kaminski A. 2009. *Nature* 457:296–300
47. Devereaux TP, Hackl R. 2007. *Rev. Mod. Phys.* 79:175–233
48. Pushp A, Parker CV, Pasupathy AN, Gomes KK, Ono S, et al. 2009. *Science* 324:5935–39

49. He RH, Tanaka K, Mo SK, Sasagawa T, Fujita M, et al. 2009. *Nat. Phys.* 5:119–23
50. Krasnov VM, Yurgens A, Winkler D, Delsing P, Claeson T. 2000. *Phys. Rev. Lett.* 84:5860–63
51. He RH, Hashimoto M, Karapetyan H, Koralek JD, Hinton JP, et al. 2011. *Science* 331:1579–83
52. Vishik IM, Nowadnick EA, Lee WS, Shen ZX, Moritz B, et al. 2009. *Nat. Phys.* 5:718–21
53. Svistunov VM, Tarenkov VY, Dyachenko AI, Hatta E. 2000. *JETP Lett.* 71:289–92
54. Renner C, Revaz B, Genoud JY, Kadowaki K, Fischer O. 1998. *Phys. Rev. Lett.* 80:149–52
55. Hashimoto M, He RH, Tanaka K, Testaud JP, Meevasana W, et al. 2010. *Nat. Phys.* 6:414–18
56. Doiron-Leyraud N, Proust C, LeBoeuf D, Levallois J, Bonnemaison JB, et al. 2007. *Nature* 447:565–68
57. Yelland EA, Singleton J, Mielke CH, Harrison N, Balakirev FF, et al. 2008. *Phys. Rev. Lett.* 100:047003
58. Meng J, Liu G, Zhang W, Zhao L, Liu H, et al. 2009. *Nature* 462:335–38
59. Yang HB, Rameau JD, Johnson PD, Valla T, Tsvelik A, Gu GD. 2008. *Nature* 456:77–80
60. King P, Rosen JA, Meevasana W, Tamai A, Rozbicki E, et al. 2011. *Phys. Rev. Lett.* 106:127005
61. Wang Y, Li L, Ong NP. 2006. *Phys. Rev. B* 73:024510
62. Li L, Wang Y, Komiya S, Ono S, Ando Y, et al. 2010. *Phys. Rev. B* 81:054510
63. Orenstein J, Corson J, Oh S, Eckstein J. 2006. *Ann. Phys.* 15:596–605
64. Grbić MS, Barišić N, Dulčić A, Kupčić I, Li Y, et al. 2009. *Phys. Rev. B* 80:094511
65. Maeno Y, Hashimoto H, Yoshida K, Nishizaki S, Fujita T, et al. 1994. *Nature* 372:532–34
66. Nagamatsu J, Nakagawa N, Muranaka T, Zenitani Y, Akimitsu J. 2001. *Nature* 410:63–64
67. Takada K, Sakurai H, Takayama-Muromachi E, Izumi F, Dilanian RA, Sasaki T. 2003. *Nature* 422:53–55
68. Kamihara Y, Watanabe T, Hirano M, Hosono H. 2008. *J. Am. Chem. Soc.* 130:3296–97
69. Ren ZA, Lu W, Yang J, Yi W, Shen XL, et al. 2008. *Chin. Phys. Lett.* 25:2215–16
70. de la Cruz C, Huang Q, Lynn JW, Li J, Ratcliff W II, et al. 2008. *Nature* 453:899–902
71. Huang Q, Qiu Y, Bao W, Green MA, Lynn JW, et al. 2008. *Phys. Rev. Lett.* 101:257003
72. Rotter M, Tegel M, Johrendt D. 2008. *Phys. Rev. Lett.* 101:107006
73. Chu JH, Analytis JG, Kucharczyk C, Fisher IR. 2009. *Phys. Rev. B* 79:014506
74. Ni N, Bud'ko SL, Kreyssig A, Nandi S, Rustan GE, et al. 2008. *Phys. Rev. B* 78:014507
75. Singh DJ, Du MH. 2008. *Phys. Rev. Lett.* 100:237003
76. Cao C, Hirschfeld PJ, Cheng HP. 2008. *Phys. Rev. B* 77:220506
77. Haule K, Shim JH, Kotliar G. 2008. *Phys. Rev. Lett.* 100:226402
78. Yin ZP, Lebègue S, Han MJ, Neal BP, Savrasov SY, Pickett WE. 2008. *Phys. Rev. Lett.* 101:047001
79. Ma F, Lu ZY, Xiang T. 2008. *Phys. Rev. B* 78:224517
80. Fang C, Yao H, Tsai WF, Hu J, Kivelson SA. 2008. *Phys. Rev. B* 77:224509
81. Xu C, Müller M, Sachdev S. 2008. *Phys. Rev. B* 78:020501
82. Mazin II, Singh DJ, Johannes MD, Du MH. 2008. *Phys. Rev. Lett.* 101:057003
83. Zhang HJ, Xu G, Dai X, Fang Z. 2009. *Chin. Phys. Lett.* 26:017401
84. Raghu S, Qi XL, Liu CX, Scalapino DJ, Zhang SC. 2008. *Phys. Rev. B* 77:220503
85. Lee PA, Wen XG. 2008. *Phys. Rev. B* 78:144517
86. Lu DH, Yi M, Mo SK, Erickson AS, Analytis J, et al. 2008. *Nature* 455:81–84
87. Lu DH, Yi M, Mo SK, Analytis J, Chu JH, et al. 2008. *Phyica C* 469:452–58
88. Mackenzie AP, Maeno Y. 2003. *Rev. Mod. Phys.* 75:657–712
89. Yi M, Lu DH, Analytis JG, Chu JH, Mo SK, et al. 2009. *Phys. Rev. B* 80:024515
90. Hsieh D, Xia Y, Wray L, Qian D, Gomes K, et al. 2008. arXiv:0812.2289
91. Zabolotnyy VB, Inosov DS, Evtushinsky DV, Koitzsch A, Kordyuk AA, et al. 2009. *Nature* 457:569–72
92. Analytis JG, Andrew CMJ, Coldea AI, McCollam A, Chu JH, et al. 2009. *Phys. Rev. Lett.* 103:076401
93. Zhai H, Wang F, Lee DH. 2009. *Phys. Rev. B* 80:064517
94. Ortenzi L, Cappelluti E, Benfatto L, Pietronero L. 2009. *Phys. Rev. Lett.* 103:046404
95. Liu G, Liu H, Zhao L, Zhang W, Jia X, et al. 2009. *Phys. Rev. B* 80:134519

96. Yi M, Lu DH, Analytis JG, Chu JH, Mo SK, et al. 2009. *Phys. Rev. B* 80:174510
97. Yang LX, Zhang Y, Ou HW, Zhao JF, Shen DW, et al. 2009. *Phys. Rev. Lett.* 102:107002
98. Zhang Y, Wei J, Ou HW, Zhao JF, Zhou B, et al. 2009. *Phys. Rev. Lett.* 102:127003
99. Richard P, Nakayama K, Sato T, Neupane M, Xu YM, et al. 2010. *Phys. Rev. Lett.* 104:137001
100. Shimojima T, Ishizaka K, Ishida Y, Katayama N, Ohgushi K, et al. 2010. *Phys. Rev. Lett.* 104:057002
101. Liu C, Kondo T, Fernandes RM, Palczewski AD, Mun ED, et al. 2010. *Nat. Phys.* 6:419–23
102. He C, Zhang Y, Xie BP, Wang XF, Yang LX, et al. 2010. *Phys. Rev. Lett.* 105:117002
103. Tanatar MA, Kreyssig A, Nandi S, Ni N, Bud'ko SL, et al. 2009. *Phys. Rev. B* 79:180508
104. Chu JH, Analytis JG, De Greve K, McMahon PL, Islam Z, et al. 2010. *Science* 329:824–26
105. Yi M, Lu DH, Chu JH, Analytis JG, Sorini AP, et al. 2011. *Proc. Natl. Acad. Sci. USA* 108:6878–83
106. Zhao J, Adroja DT, Yao DX, Bewley R, Li S, et al. 2009. *Nat. Phys.* 5:555–60
107. Chuang TM, Allan MP, Lee J, Xie Y, Ni N, et al. 2010. *Science* 327:181–84
108. Mazin II, Johannes MD. *Nat. Phys.* 5:141–45
109. Lee CC, Yin WG, Ku W. 2009. *Phys. Rev. Lett.* 103:267001
110. Lv W, Krüger F, Phillips P. 2010. *Phys. Rev. B* 82:045125
111. Chen CC, Maciejko J, Sorini AP, Moritz B, Singh RRP, Devereaux TP. 2010. *Phys. Rev. B* 82:100504
112. Boeri L, Dolgov OV, Golubov AA. 2008. *Phys. Rev. Lett.* 101:026403
113. Chen TY, Tesanovic Z, Liu RH, Chen XH, Chien CL. 2008. *Nature* 453:1224–27
114. Hashimoto K, Shibauchi T, Kato T, Ikada K, Okazaki R, et al. 2009. *Phys. Rev. Lett.* 102:017002
115. Matano K, Ren ZA, Dong XL, Sun LL, Zhao ZX, et al. 2008. *Europhys. Lett.* 83:57001
116. Hicks CW, Lippman TM, Huber ME, Analytis JG, Chu JH, et al. 2009. *Phys. Rev. Lett.* 103:127003
117. Lee CH, Iyo A, Eisaki H, Kito H, Fernandez-Diaz MT, et al. 2008. *J. Phys. Soc. Jpn.* 77:083704
118. Kuroki K, Usui H, Onari S, Arita R, Aoki H. 2009. *Phys. Rev. B* 79:224511
119. Ding H, Richard P, Nakayama K, Sugawara K, Arakane T, et al. 2008. *Europhys. Lett.* 83:47001
120. Zhang Y, Yang LX, Chen F, Zhou B, Wang XF, et al. 2010. *Phys. Rev. Lett.* 105:117003
121. Xu YM, Huang YB, Cui XY, Razzoli E, Radovic M, et al. 2011. *Nat. Phys.* 7:198–202
122. Zhang Y, Ye ZR, Ge QQ, Chen F, Jiang J, et al. 2011. arXiv:1109.0229
123. Suzuki K, Usui H, Kuroki K. 2011. *J. Phys. Soc. Jpn.* 80:013710
124. Sekiba Y, Sato T, Nakayama K, Terashima K, Richard P, et al. 2009. *N. J. Phys.* 11:025020
125. Nakayama K, Sato T, Richard P, Xu YM, Kawahara T, et al. 2011. *Phys. Rev. B* 83:020501
126. Yang WL, Sorini AP, Chen CC, Moritz B, Lee WS, et al. 2009. *Phys. Rev. B* 80:014508
127. Tamai A, Ganin AY, Rozbicki E, Bacsa J, Meevasana W, et al. 2010. *Phys. Rev. Lett.* 104:097002
128. Zhang Y, Chen F, He C, Yang LX, Xie BP, et al. 2010. *Phys. Rev. B* 82:165113
129. Guo J, Jin S, Wang G, Wang S, Zhu K, et al. 2010. *Phys. Rev. B* 82:180520
130. Moon SJ, Shin JH, Parker D, Choi WS, Mazin II, et al. 2010. *Phys. Rev. B* 81:205114
131. Reid JP, Tanatar MA, Luo XG, Shakeripour H, Doiron-Leyraud N, et al. 2010. *Phys. Rev. B* 82:064501
132. Zhang Y, Yang LX, Xu M, Ye ZR, Chen F, et al. 2011. *Nat. Mater.* 10:273–77
133. Wang XP, Qian T, Richard P, Zhang P, Dong J, et al. 2011. *Europhys. Lett.* 93:57001
134. Mou D, Liu S, Jia X, He J, Peng Y, et al. 2011. *Phys. Rev. Lett.* 106:107001
135. Geim AK, Novoselov KS. 2007. *Nat. Mater.* 6:183–91
136. Neto AHC, Guinea F, Peres NMR, Novoselov KS, Geim AK. 2009. *Rev. Mod. Phys.* 81:109–62
137. Novoselov K, Geim A, Morozov S, Jiang D, Katsnelson M, et al. 2005. *Nature* 438:197–200
138. Zhang Y, Tan Y, Stormer H, Kim P. 2005. *Nature* 438:201–4
139. Wallace P. 1947. *Phys. Rev.* 71:622–34
140. Semenoff G. 1984. *Phys. Rev. Lett.* 53:2449–52
141. Berger C, Song Z, Li X, Wu X, Brown N, et al. 2006. *Science* 312:1191–95
142. Divincenzo D, Mele E. 1984. *Phys. Rev. B* 29:1685–94
143. Novoselov K, Geim A, Morozov S, Jiang D, Zhang Y, et al. 2004. *Science* 306:666–69
144. Morozov S, Novoselov K, Schedin F, Jiang D, Firsov A, Geim A. 2005. *Phys. Rev. B* 72:201401
145. Hebard A, Rosseinsky M, Haddon R, Murphy D, Glarum S, et al. 1991. *Nature* 350:600–1
146. Tang Z, Zhang L, Wang N, Zhang X, Wen G, et al. 2001. *Science* 292:2462–65

147. Kociak M, Kasumov A, Gueron S, Reulet B, Khodos I, et al. 2001. *Phys. Rev. Lett.* 86:2416–19
148. Hannay N, Geballe T, Matthias B, Andres K, Schmidt P, Macnair D. 1965. *Phys. Rev. Lett.* 14:225–26
149. Weller T, Ellerby M, Saxena S, Smith R, Skipper N. 2005. *Nat. Phys.* 1:39–41
150. Reich S, Maultzsch J, Thomsen C, Ordejon P. 2002. *Phys. Rev. B* 66:035412
151. Saito R, Dresselhaus G, Dresselhaus M. 1998. *Physical Properties of Carbon Nanotubes*. London: Imp. Coll. Press
152. Bostwick A, Ohta T, Seyller T, Horn K, Rotenberg E. 2007. *Nat. Phys.* 3:36–40
153. Sprinkle M, Siegel D, Hu Y, Hicks J, Tejeda A, et al. 2009. *Phys. Rev. Lett.* 103:226803
154. Zhou SY, Gweon GH, Fedorov AV, First PN, De Heer WA, et al. 2007. *Nat. Mater.* 6:770–75
155. Zhou SY, Siegel DA, Fedorov AV, Lanzara A. 2008. *Phys. Rev. B* 78:193404
156. Novoselov K, Jiang D, Schedin F, Booth T, Khotkevich V, et al. 2005. *Proc. Natl. Acad. Sci. USA* 102:10451–53
157. Varykhalov A, Sanchez-Barriga J, Shikin AM, Biswas C, Vescovo E, et al. 2008. *Phys. Rev. Lett.* 101:157601
158. Sutter PW, Flege JI, Sutter EA. 2008. *Nat. Mater.* 7:406–11
159. Rollings E, Gweon GH, Zhou SY, Mun BS, McChesney JL, et al. 2006. *J. Phys. Chem. Solids* 67:2172–77
160. Ohta T, Bostwick A, Seyller T, Horn K, Rotenberg E. 2006. *Science* 313:951–54
161. Lounis SD, Siegel DA, Broesler R, Hwang CG, Haller EE, Lanzara A. 2010. *Appl. Phys. Lett.* 96:151913
162. Siegel DA, Hwang CG, Fedorov AV, Lanzara A. 2010. *Phys. Rev. B* 81:241417
163. Ohta T, Bostwick A, McChesney JL, Seyller T, Horn K, Rotenberg E. 2007. *Phys. Rev. Lett.* 98:206802
164. Bostwick A, Speck F, Seyller T, Horn K, Polini M, et al. 2010. *Science* 328:999–1002
165. Zhou SY, Siegel DA, Fedorov AV, Lanzara A. 2008. *Phys. Rev. Lett.* 101:086402
166. Bostwick A, McChesney JL, Emtsev KV, Seyller T, Horn K, et al. 2009. *Phys. Rev. Lett.* 103:056404
167. Rotenberg E, Bostwick A, Ohta T, McChesney JL, Seyller T, Horn K. 2008. *Nat. Mater.* 7:258–59
168. Zhou SY, Siegel DA, Fedorov AV, Lanzara A. 2008. *Physica E* 40:2642–47
169. Bostwick A, Ohta T, McChesney JL, Emtsev KV, Seyller T, et al. 2007. *N. J. Phys.* 9:385
170. Sutter P, Hybertsen MS, Sadowski JT, Sutter E. 2009. *Nano Lett.* 9:2654–60
171. Enderlein C, Kim YS, Bostwick A, Rotenberg E, Horn K. 2010. *N. J. Phys.* 12:033014
172. Moos G, Gahl C, Fasel R, Wolf M, Hertel T. 2001. *Phys. Rev. Lett.* 87:267402
173. McChesney JL, Bostwick A, Ohta T, Seyller T, Horn K, et al. 2010. *Phys. Rev. Lett.* 104:136803
174. Emtsev KV, Bostwick A, Horn K, Jobst J, Kellogg GL, et al. 2009. *Nat. Mater.* 8:203–7
175. Anderson PW. 1997. *Basic Notions of Condensed Matter Physics*. New York: Westview Press
176. Kv K, Dorda G, Pepper M. 1980. *Phys. Rev. Lett.* 45:494–97
177. Qi XL, Zhang SC. 2010. *Phys. Today* 63:33–38
178. Bernevig BA, Hughes TL, Zhang SC. 2006. *Science* 314:1757–61
179. König M, Wiedmann S, Brne C, Roth A, Buhmann H, et al. 2007. *Science* 318:766–70
180. Kane CL, Mele EJ. 2005. *Phys. Rev. Lett.* 95:226801
181. Bernevig BA, Zhang SC. 2006. *Phys. Rev. Lett.* 96:106802
182. Kane CL, Mele EJ. 2005. *Phys. Rev. Lett.* 95:146802
183. Fu L, Kane CL, Mele EJ. 2007. *Phys. Rev. Lett.* 98:106803
184. Moore JE, Balents L. 2007. *Phys. Rev. B* 75:121306
185. Qi XL, Hughes TL, Zhang SC. 2008. *Phys. Rev. B* 78:195424
186. Roy R. 2009. *Phys. Rev. B* 79:195321
187. Fu L, Kane CL. 2007. *Phys. Rev. B* 76:045302
188. Zhang H, Liu CX, Qi XL, Dai X, Fang Z, Zhang SC. 2009. *Nat. Phys.* 5:438–42
189. Yan B, Liu CX, Zhang HJ, Yam CY, Qi XL, et al. 2010. *Europhys. Lett.* 90:37002
190. Lin H, Markiewicz RS, Wray LA, Fu L, Hasan MZ, Bansil A. 2010. *Phys. Rev. Lett.* 105:036404
191. Chadov S, Qi X, Kuebler J, Fecher GH, Felser C, Zhang SC. 2010. *Nat. Mater.* 9:541–45
192. Lin H, Wray LA, Xia Y, Xu S, Jia S, et al. 2010. *Nat. Mater.* 9:546–49

193. Hsieh D, Qian D, Wray L, Xia Y, Hor YS, et al. 2008. *Nature* 452:970–74
194. Hsieh D, Xia Y, Wray L, Qian D, Pal A, et al. 2009. *Science* 323:919–22
195. Chen YL, Analytis JG, Chu JH, Liu ZK, Mo SK, et al. 2009. *Science* 325:178–81
196. Xia Y, Qian D, Hsieh D, Wray L, Pal A, et al. 2009. *Nat. Phys.* 5:398–402
197. Hsieh D, Xia Y, Qian D, Wray L, Meier F, et al. 2009. *Phys. Rev. Lett.* 103:146401
198. Chen YL, Chu JH, Analytis JG, Liu ZK, Igarashi K, et al. 2010. *Science* 329:659–62
199. Fu L. 2009. *Phys. Rev. Lett.* 103:266801
200. Alpichshev Z, Analytis JG, Chu JH, Fisher IR, Chen YL, et al. 2010. *Phys. Rev. Lett.* 104:016401
201. Hsieh D, Xia Y, Qian D, Wray L, Dil JH, et al. 2009. *Nature* 460:1101–5
202. Qi XL, Li R, Zang J, Zhang SC. 2009. *Science* 323:1184–87
203. Zang J, Nagaosa N. 2010. *Phys. Rev. B* 81:245125
204. Wilczek F. 2009. *Nature* 458:129
205. Analytis JG, Chu JH, Chen Y, Corredor F, McDonald RD, et al. 2010. *Phys. Rev. B* 81:205407
206. Chen YL, Liu ZK, Analytis JG, Chu JH, Zhang HJ, et al. 2010. *Phys. Rev. Lett.* 105:266401
207. Hein RA, Swiggard EM. 1970. *Phys. Rev. Lett.* 24:53–55
208. Qi XL, Hughes TL, Raghu S, Zhang SC. 2009. *Phys. Rev. Lett.* 102:187001
209. Nayak C, Simon SH, Stern A, Freedman M, Das Sarma S. 2008. *Rev. Mod. Phys.* 80:1083–159
210. Yu R, Zhang W, Zhang HJ, Zhang SC, Dai X, Fang Z. 2010. *Science* 329:61–64
211. Wilczek F. 2009. *Nat. Phys.* 5:614–18
212. Hor Y, Checkelsky J, Qu D, Ong N, Cava R. 2010. *J. Phys. Chem. Solids* 72:572–76
213. Qi XL, Hughes TL, Zhang SC. 2010. *Phys. Rev. B* 81:134508
214. Schnyder AP, Ryu S, Furusaki A, Ludwig AWW. 2008. *Phys. Rev. B* 78:195125